Melt Fracture, Melt Viscosities, and Die Swell of Polypropylene Resin in Capillary Flow

Jan-Chan Huang, Zhenghong Tao

Department of Plastics Engineering, University of Massachusetts Lowell, Lowell, Massachusetts 01854

Received 19 February 2002; accepted 20 May 2002

ABSTRACT: The melt fracture, shear viscosity, extensional viscosity, and die swell of a polypropylene resin were studied using a capillary rheometer and dies with a 0.05-cm diameter and length/radius ratios of 10, 40, and 60. A temperature of 190°C and shear rates between 1 and 5000 s^{-1} were used. A modified Bagley plot was used with consideration of pressure effects on both the melt viscosity and end effect. The shear viscosity was calculated from the true wall shear stress. When the true wall shear stress increased, the end effect increased and showed critical stresses at around 0.1 and 0.17 MPa. The extensional viscosity was calculated from the end effect and it showed a decreasing trend when the strain rate increased. Both the shear and extensional viscosities correlated well with another polypropylene reported previously. The die swell was higher for shorter dies and increased when shear stress increased. When the shear rates increased, the extrudate changed from smooth to gross melt fracture with regular patterns (spurt) and then turned into an irregular shape. In the regular stage the wavelength of the extrudates increased when the shear rate increased. The frequency of melt fracture was almost independent of the shear rate, but it decreased slightly when the die length increased. © 2002 Wiley Periodicals, Inc. J Appl Polym Sci 87: 1587–1594, 2003

Key words: capillary rheometer; shear viscosity; extensional viscosity; polypropylene; die swell; melt fracture

INTRODUCTION

The flow behavior of polymer melts is of great practical importance in the design of polymer processing equipment. The upper limit of the processing rate of a polymer is frequently limited by the occurrence of melt fracture phenomena. The term melt fracture is used to generally describe extrudate distortion or the variation of the shape of the extrudate. Melt fracture is a flow instability phenomenon occurring when a polymer melt is extruded through a capillary at rates exceeding a critical shear stress.[1–20] Most of the previous studies on the melt fracture of polymers focused on the behavior of various types of polyethylenes (PEs: high density, low density, and linear low density).[1–10] The melt fracture of PE is complicated. Sornberger et al.[1] divided the flow curve of linear PE into five stages. In the first stage a smooth cylindrical extrudate is seen at low shear rates. In the second stage, when the flow rate is increased, the extrudate develops a small-amplitude high-frequency disturbance on its surface, which is called sharkskin. This is also known as surface melt fracture. As the flow rate is increased in the third stage, a pressure oscillation can be observed for a constant flow system. The flow is sometimes called a spurt flow and has been interpreted by the slip-stick phenomenon near the capillary surface,[1–6] compressibility of polymer melts,[7] combination of slip and compressibility,[8,9] or constitutive instability of polymer melts.[10] A periodical pattern may appear on the extrudates. This is also called regular melt fracture in this article. The frequency at this stage is lower than the frequency in sharkskin. The frequency is on the order of 1 s^{-1}, while sharkskin can have a frequency on the order of 100 s^{-1}. If the flow is at constant pressure, a flow curve hysteresis with two different possible flow rates can be observed. This is accompanied by a discontinuity in the plot of the flow rate versus the pressure drop. When increasing the shear rate further, a relatively smooth extrudate is observed in the fourth stage. Finally, in the fifth stage, a very disordered lump called a wavy melt fracture is observed at the even higher flow rate.

Polypropylene (PP) is a material of great industrial importance, because it has found many applications in fiber, injection molding, and film production. The melt fracture of PP was studied in the literature. It is simpler than that of PE. In particular, no sharkskin and discontinuity in flow curve were observed. Ui et al.[12] reported continuous smooth curves without discontinuity for PP. At 180°C the shape of the obtained fractured extrudate surface was fairly regular. They also noted that the wavelengths of the regular melt fracture increased as the shear rate increased and that at higher shear rates perfectly smooth extrudates were obtained. When the shear rate was increased even

Correspondence to: J.-C. Huang (Jan_Huang@uml.edu).

Journal of Applied Polymer Science, Vol. 87, 1587–1594 (2003)

more, a second sharp roughness appeared on the surface of the extrudate. They reported that melt fracture occurred at a critical wall shear stress value in the range of 0.1–0.13 MPa, independent of the temperature in the 180–260°C range. Ballenger et al.[13] also reported that the extrudate shape changed from smooth to pitched screw threads to smooth and finally to a distorted form as the shear rate increased. Bartos[14] studied the melt fracture behavior of a series of PPs to examine the critical conditions for the onset of extrudate distortions. He found that melt fracture occurred at a wall shear stress in the range of 0.069–0.16 MPa. Kamide et al.[15] also studied PP flow and reported a critical wall shear stress value of 0.11 MPa. Other work addressing the melt fracture of PP includes Akay[16] and Fujiyama and Kawasaki.[17] They reported critical shear stresses for the onset of melt fracture ranging from 0.13 to 0.2 MPa.

The purpose of this article was to study the shear viscosity, extensional viscosity, die swell, and melt fracture of a high molecular weight PP in capillary flow. Three die lengths were used to observe the effect of die length. A similar study was made on an injection molding grade PP with a lower molecular weight.[18]

EXPERIMENTAL

The material used in this study was Atofina 3181 PP resin. It is a commercial grade homopolymer for sheet and strapping applications and contains additives to prevent oxidation and degradation during processing. It has a melt flow index of 0.75 g/10 min as measured by ASTM D1238 condition L. The number-average molecular weight (M_n) was 84,000 and the weight-average molecular weight (M_w) was 512,000. This information was provided by the company manufacturing it. The rheological properties were measured on a Galaxy V capillary rheometer (model 8025, Kayness Inc.) equipped with a computer for data acquisition. The pressure sensor of the capillary rheometer was located at the capillary entrance. Three tungsten carbide capillaries with a flat entrance region were used. The diameter was 0.10 cm and the die lengths were 0.50, 2.0, and 3.0 cm. These gave length to radius (L/R) ratios of 10, 40, and 60, respectively. Eighteen shear rates from 1 to 5000 s^{-1} were used. A temperature of 190°C was chosen for this study.

RESULTS AND DISCUSSION

The melt fracture of PP was observed from the extrudates. When melt fracture occurred the extrudate no longer maintained a smooth cylindrical geometry. Figure 1 shows the extrudates of the shortest die collected at 190°C. The melt fracture became noticeable when the apparent shear rates exceeded 100 s^{-1}. It was also observed that regular patterns appeared on extrudates between 100 and 1000 s^{-1}. At even higher shear rates the extrudate showed an irregular pattern. Within the shear rate ranges of this study there was no second smooth extrudate. When melt fracture appeared as a periodical pattern, the wavelength was also measured. As the die length increased the start of a regular pattern was delayed to a higher shear rate. It was also noted that when the shear rate increased, the wavelength increased. The pattern of regular melt fracture appeared to be different from those reported by Baik and Tzogankis[19] and Kazatchkov et al.[20] In their studies regular helixlike extrudates were observed between 700 and 5000 s^{-1}. A smooth extrudate was observed between 6000 and 10,000 s^{-1}. At 20,000 s^{-1} and higher, irregular extrudates were observed. In our study the shear rate range for regular melt fracture was narrower, and more complicated extrudates were obtained starting at a shear rate of 200 s^{-1}. The extrudates contained globelike lumps and were not of constant diameter.

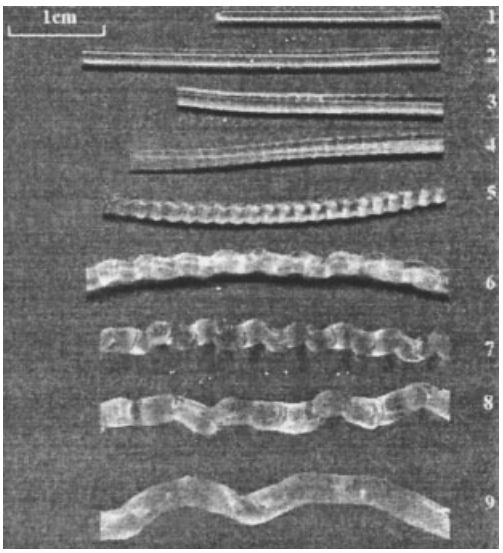

Figure 1 The melt fracture of Atofina 3429 at 190°C and a die length of 10 mm. From top to bottom the apparent shear rates are 5, 20, 100, 120, 200, 800, 1000, 2000, and 5000, respectively.

Figure 2 shows the apparent shear stress ($\tau_a = R\Delta P/2L$) versus the apparent shear rate ($\dot{\gamma}_a = 4Q/R^3$, Q is the volume flow rate) for the three dies. This plot was commonly used to identify the existence of melt fracture and wall slip.[1–4] When a melt fracture occurred, the plot could have a discontinuity. No such phenomenon was seen in this study. It was noted that there were two breaks in the slopes in the curves in Figure 2, which are marked by arrows. This is typical for melt fracture of PP. Kazatchkov et al.[20] and Ui et al.[12] also reported breaks similar to our observation. The lower one corresponded to the inception of the regular melt fracture and the higher one corresponded to the be-

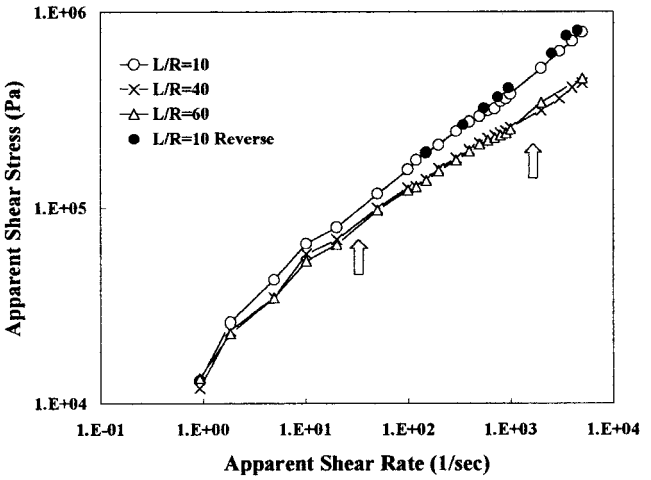

Figure 2 The apparent shear stress versus the apparent shear rate for three die lengths.

ginning of the irregular melt fracture. To observe any flow hysteresis phenomena, a pressure versus flow rate measurement was also made in the reverse direction, starting from high flow rates and going down to low flow rates. The results of both types of measurements overlapped well and suggested that there was no flow hysteresis.

Both the apparent shear stress and apparent shear rate increased in tandem in Figure 2, but at the high shear rate region the slope was lower than at the low shear rate region. This is typical for a material exhibiting a shear thinning phenomenon. The curves of the two longer capillary dies overlapped with each other and had lower shear stress than the shortest die at a given shear rate value. Furthermore, the distance separating the curve of $L/R = 10$ and the other two widened when the apparent shear rates and apparent shear stresses increased. This indicated the existence of pressure effects on the shear viscosity and end effects, which became more significant at a higher barrel pressure.

When the pressure drop of each flow rate was plotted versus L/R, an upward trend was observed as in a previous study.[18] This was explained by the pressure dependence of the shear and extensional viscosities. The following function is used to describe the effect of pressure on the shear viscosity[18–24]:

$$\eta = \eta_0 e^{\beta P} \tag{1}$$

where η_0 is the shear viscosity at zero pressure and β is the pressure coefficient. A similar expression has also been used to describe the pressure dependency on the extensional viscosity[18,25,26]:

$$\eta_e = \eta_{e,0} e^{\alpha P} \tag{2}$$

where $\eta_{e,0}$ is the extensional viscosity at zero pressure and α is the pressure coefficient.

Without pressure effects on the viscosity, the plot of the pressure drop versus the die length is a straight line. This is the well-known Bagley plot[27]:

$$\Delta P = 2\tau_{tw}(L/R + e) \tag{3}$$

The calculation of the shear viscosity started from a plot of the true wall shear stress (τ_{tw}) versus the apparent shear rate ($\dot{\gamma}_a$) on a double logarithm scale. The slope n of this plot was used to make the Rabinowitsch correction. The Rabinowitsch correction was made to calculate the true shear rate on the capillary surface ($\dot{\gamma}_{tw}$) from the $\dot{\gamma}_a$:

$$\dot{\gamma}_{tw} = \dot{\gamma}_a(3n + 1)/4n \tag{4}$$

With the true shear rate, the shear viscosity was calculated as

$$\eta = \tau_{tw}/\dot{\gamma}_{tw} \tag{5}$$

Using eq. (1) as the pressure dependence of the shear viscosity, the following relation between the pressure drop and die length was derived by integration of the momentum equation[18,22]:

$$[1 - \exp(-\beta\Delta P)]/\beta = 2\tau(L/R + e) \tag{6}$$

The left side of the above equation reduces to ΔP when β is small. It was also derived by Denn[24] in an analysis of adiabatic flow with the pressure dependence of the viscosity.

The effect of pressure on the extensional viscosity is included in the end effect. From the end effect, the $\eta_{e,o}$ as a function of the extensional rate ($\dot{\varepsilon}$) can be calculated based on the equations derived by Cogswell.[28] In his analysis it was assumed that the polymer melt adopts a conicylindrical flow pattern as it passes from the reservoir into the capillary and that this pattern corresponds to a minimum entrance pressure drop. It was also assumed that the shear viscosity of the polymer melt could be described in terms of a Power law model. Following this analysis, the extensional viscosity and the extensional strain rate may be calculated as

$$\eta_e(\dot{\varepsilon}) = \frac{9}{32}\frac{(n + 1)^2\Delta P_e^2}{\eta(\dot{\gamma}_a)\dot{\gamma}_a^2} \tag{7}$$

$$\dot{\varepsilon} = \frac{4}{3}\frac{\eta(\dot{\gamma}_a)\dot{\gamma}_a^2}{(n + 1)\Delta P_e} \tag{8}$$

where n is the Power law exponent, ΔP_e is the entrance pressure drop corresponding to a zero capillary die length, η is the shear viscosity, and $\dot{\gamma}_a$ is as previously.

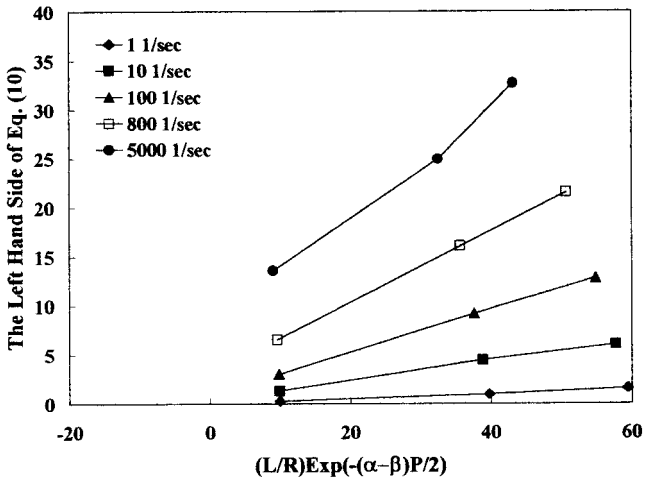

Figure 3 The left-hand side of eq. (10) versus $(L/R)\exp[-(\alpha - \beta)P/2]$ for selected apparent shear rates.

Using the relation between the entrance pressure drop and the end effect, $\Delta P_e = 2e\tau_{tw} = 2e\eta(\dot{\gamma}_a)\dot{\gamma}_a$, eq. (7) can be changed to

$$e = \frac{2\sqrt{2}}{3(1+n)}\sqrt{\eta_e(\dot{\varepsilon})/\eta(\dot{\gamma})} \tag{9}$$

It can be seen that the pressure dependence of the end effect depends on the pressure dependence of both η_e and η. Therefore, the end effect can be separated into a product of the zero pressure component E and its pressure dependency. Based on eq. (9), the dependence of the end effect on pressure is one-half of the ratio of the dependence between the extensional viscosity and shear viscosity: $e = E\exp[(\alpha - \beta)\Delta P/2]$. The ΔP is the barrel pressure where the end effect took place. This approach was used in our previous article,[18] but the relationship was mistakenly used as $e = E\exp(\alpha\Delta P)$. After separating the end effect into E and the pressure dependent term, the following equation is obtained:

$$[1 - \exp(-\beta\Delta P)]\exp[-(\alpha - \beta)\Delta P/2]/\beta = 2\tau_{tw}\{(L/R)\exp[-(\alpha - \beta)\Delta P/2] + E\} \tag{10}$$

Here τ_{tw} is the true wall shear stress and E is the end effect, both at zero pressure. When values of α and β are small, eq. (10) reduces to the Bagley equation. If parameters α and β are known, the left-hand side of eq. (10) can yield a linear plot versus $(L/R)\exp[-(\alpha - \beta)\Delta P/2]$.

Recently, Bindings et al.[25] determined the pressure dependency of the shear viscosity and extensional viscosity of several polymers using a capillary rheometer that could be pressurized at both the inlet and outlet. It turned out that the pressure dependency of the extensional viscosity was higher than the shear viscosity for PP, PE, poly(methyl methacrylate), and polystyrene. Christensen and Kjaer[26] also used capillary dies with zero die length to measure the effect of pressure on the end effect. The values of α and β obtained by Binding et al.[25] were used in this study. The values of α and β were 19.1 and 7.1 GPa^{-1}, respectively. Figure 3 shows the left-hand side of eq. (3) versus $(L/R)\exp[-(\alpha - \beta)\Delta P/2]$ for selected apparent shear rates. The curves for the apparent shear rate between 2000 and 5000 s^{-1} still showed an upward trend. This was because between those shear rates the extrudate entered the irregular melt fracture stage. The curves for the shear rate below 2000 s^{-1} showed linear trends. From a linear regression calculation the values of τ_{tw} and E were determined. From eqs. (4) and (5) the shear viscosity was calculated. The extensional viscosity was calculated using eqs. (7) and (10). Both viscosities were at zero pressure.

Kazatchkov et al.[20] observed the melt distortion of a PP resin in both capillary and slit dies. Several diameters and slit thicknesses were used. The flow curves, determined by using capillaries having various diameters, were independent of the diameter, implying the absence of slip. However, experiments with rough-surface slit dies suggested wall slip. As a result, they suggested that the possibility of slip existed in the capillary die at a high shear rate region. The critical shear stress for the slip was determined to be 0.13 MPa. This shear stress corresponds to the apparent shear rate of about 150 s^{-1} in our study and coincides with the appearance of visible melt fracture. In view of the conclusion of Kazatchkov et al.,[20] the melt viscosities in the melt fracture region should be used with caution, because wall slip can change the trend of the results.

Figure 4 presents the results of the shear viscosity of Atofina 3181. It shows a strong shear rate dependency in the shear rate region studied, which justified the use of the Rabinowitsch correction. At the low end of the

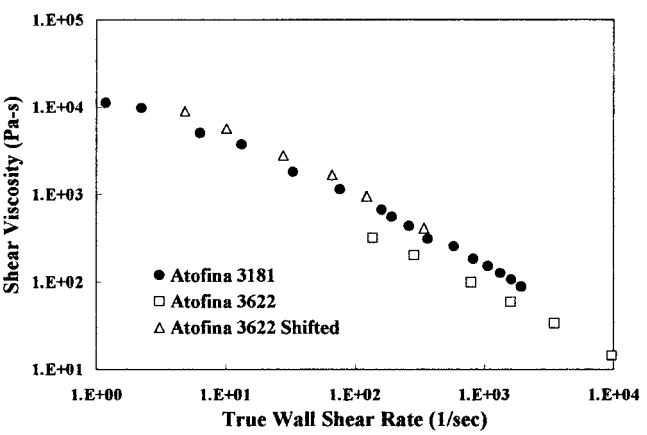

Figure 4 The shear viscosity of Atofina 3181 and Atofina 3622.

shear rates, the melt viscosity had not reached the Newtonian region. This indicated that the material had a broad molecular weight distribution, which was reported by the manufacturer to be 6.1. Also shown in Figure 4 is the results of Atofina 3622 measured earlier[18] but corrected using eq. (10) of this study. The shear viscosity of Atofina 3181 was higher than Atofina 3622. At the high shear rate, the Power law exponent of Atofina 3181 was estimated to be 0.16, which was higher than the value of 0.23 for Atofina 3622 because the former had a higher molecular weight. It was noted that, despite the occurrence of melt fracture, the viscosity results still showed a continuous trend. This indicated that, in both regular and irregular melt fracture, the increase of pressure drop was constant and was separated from the wall shear stress in the linear plot of eq. (10). This also suggested that the energy loss in the melt fracture of PP was independent of the die length and was likely to be associated with the entrance effect or created at the die exit similar to the sharkskin of PE.[29]

The melt viscosity results of polymers with different molecular weights can be superimposed with proper adjustment of the parameters. A superposition can be made for the shear viscosity based on the following formula[30]:

$$\eta/\eta_0 = f(\lambda\dot{\gamma}) \tag{11}$$

where η_0 is the Newtonian viscosity and γ is the relaxation time. If the Newtonian viscosity and time constant are similar functions of the M_w, the following equation can be obtained:

$$\eta(\dot{\gamma}/a_T) = a_T\eta(\dot{\gamma}) \tag{12}$$

where the shift factor $a_T = \eta_{0,1}/\eta_{0,2}$ adjusts the effect of the molecular weight. This equation predicts a master shear viscosity curve, if the viscosity is multiplied by the ratio of their Newtonian viscosities and the shear rate is divided by the same ratio. Because the M_w of both PPs exceeded the critical molecular weight for entanglement (7000),[31] the shift factor was proportional to the 3.4 power of the M_w.[32] The value was calculated to be 28.37 using PP 3181 as polymer 1 and PP 3622 as polymer 2. The result of the superposition adjustment is shown in Figure 4. It can be seen that both PPs overlapped well after the shift data. This indicated that both polymers had similar rheological behaviors and molecular weight distributions.

The end effect at zero pressure E is plotted versus the true wall shear stress in Figure 5. The results of the end effect showed that there were two transitions, separating the data into three zones. One transition occurred near 0.1 MPa and the other at 0.17 MPa. The former corresponded to the start of the regular melt fracture, while the second critical shear stress corresponded to the transition to an irregular melt fracture. At the stress below the first critical stress, the end effect increased slowly when the stress increased. Between the first and second critical shear stresses the end effect increased at a higher rate. During this stage the trend of the end effect of Atofina 3181 was very similar to that of Atofina 3362 reported earlier,[18] despite the fact that the shear viscosity of the former was about 3 times higher than the latter. Several authors have studied the critical stress of melt fracture of PP based on the observation of extrudates.[12–20] In particular, Baik and Tzoganakis[19] studied the melt fracture of a series of PPs prepared by peroxide oxidation. The critical stress was found to decrease linearly from 0.15 to 0.10 MPa when the M_w increased from 100,000 to 400,000. Because the molecular weight of PP used in this study was higher than the above critical stress range, the occurrence of melt fracture was expected to be at the lower end of the above critical stress range, which agreed with Figure 5. It is interesting to point out that the increase in the end effect was not significant until the onset of irregular melt fracture. This indicated that, in the regular melt fracture stage, the energy loss was not significantly increased yet. In the irregular stage of a melt fracture phenomenon, the energy loss increases much more quickly and is manifested as a sharp increase of the end effect. In a previous article on a metallocene copolymer of ethylene and octene[23] it was also observed that the visible melt fracture started at a lower shear stress, but a large increase in the end effect occurred at a higher shear stress.

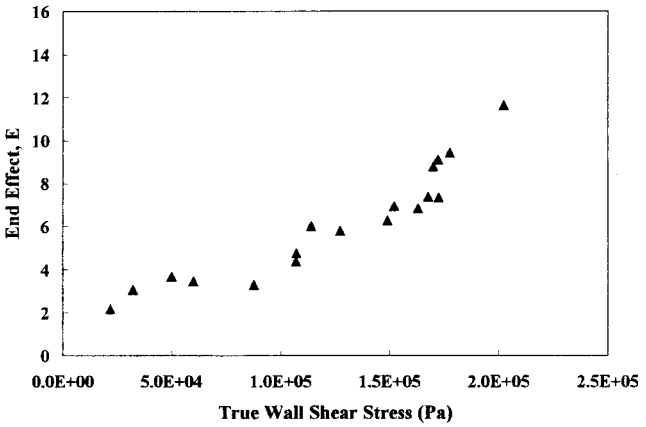

Figure 5 The end correction versus the true wall shear stress of Atofina 3181.

The results for the extensional viscosity are shown in Figure 6. The plot is similar to the extensional viscosity of Atofina 3622,[18] which was also calculated by the approach in this article. The values of Atofina 3181 were about 8 times the values of Atofina 3622 at a given extensional rate. This was higher than their shear viscosities. This was because the range of strain

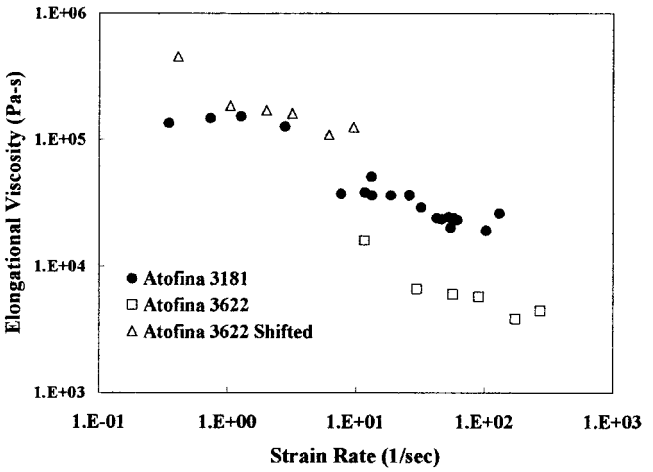

Figure 6 The extensional viscosity versus the extensional strain rate of Atofina 3181 and Atofina 3622.

rates was 10 times lower than the corresponding shear rate. As the Newtonian region was approached, the distance separating the two curves widened. The extensional viscosity of a series of PPs was measured by Tzoganakis et al.[33] using eqs. (7) and (8). The extensional viscosity of a sample with M_w = 200,000 was about 3000 Pa s at 100 s^{-1}. This agreed with our results for Atofina 3633. The molecular weight of Atofina 3181 exceeded the range of PPs studied by Tzoganakis et al.[33] A shift similar to the shear viscosity can be made to compare the extensional viscosity of PP with different molecular weights. The results are also shown in Figure 6. It can be seen that, after the shift, the results of both PPs overlapped very well. At the low strain rate, the extensional viscosity decreased as a Power law function when the strain rate increased. It is interesting that the data corresponding to the regular melt fracture still followed the trend. At the strain rate corresponding to the irregular melt fracture, the data became nearly horizontal. This deviation from the trend originated from the high values of the end correction after the second critical shear stresses. A high value for the end correction could be attributed to the melt fracture phenomena, which formed another source of pressure drop and end effect. A comparison of eqs. (7) and (8) showed that an increase in ΔP_e increases the η_e at twice the rate it decreases $\dot{\epsilon}$. Therefore, the data at a high shear rate tended to deviate upward and with a smaller slope. In this situation, the formula for the extensional viscosity was no longer applicable. Only the low strain rate region of Atofina 3181 provided the same basis for comparison.

The die swell (B) was measured as the ratio of the solid extrudate diameter (D_{ex}) to the diameter of the die (D) and corrected by the density ratio between 190°C and room temperature using the equation

$$B = (D_{ex}/D) \times (\text{Density at room temp})/(\text{Density at 190°C}).$$

The density values of a PP at room temperature and melt temperatures from Zoller and Walsh[34] were used. When melt fracture occurred, the diameter was measured at several locations and an average was taken. As seen in Figure 1, the diameter variation in the regular melt fracture was higher than the irregular melt fracture, which was near the onset of second smooth extrudates. It was noted that the die swell and severity of the melt fracture decreased when the die length increased, which agreed with the observation of Ballenger et al.[13] This showed that the relaxation process took place in longer dies. The draw-down by gravity was smaller than the previous study,[18] because of the higher melt viscosity in this study. The die swell of Atofina 3181 is shown in Figure 7. It can be seen that the die swell increased quickly after the onset of visible die swell. Two critical shear stresses were observed at (1.0 and 1.5) $\times$ 10^5 Pa, which were similar to the end effect observation.

Vlachopoulos[35] suggested that die swell contained four components: Newtonian, elastic, inelastic, and relax. The contribution of the Newtonian is taken to be a constant value of 0.12, and the inelastic and relax components are considered small in some cases. The majority contribution of die swell is the elastic component, but at low shear rate the die swell ratio is 1.12. In our study the die swell at the low shear stress was close to the value of 1.12 as seen in Figure 7. Die swell results were reported by Tzoganakis et al.[33] and Brandao et al.[36] The former study showed the effect of annealing on the die swell results. Without annealing, the die swell was about 1.6 at a shear rate of 100 kPa. After annealing the result was 2.1. When compared with preannealing data, our results on the longest die were close to the results of Tzoganakis et al.[33]

For PE, surface melt fracture (sharkskin) usually occurs before gross melt fracture.[1–8] However, this type of distortion did not occur in the case of PP.[12–17]

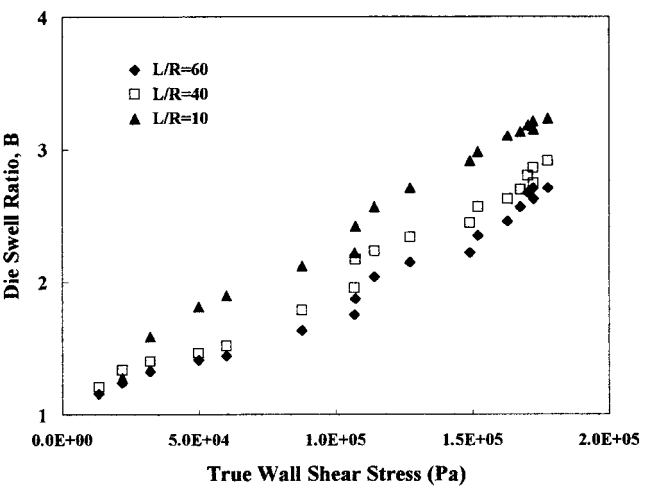

Figure 7 The die swell ratio of Atofina 3181.

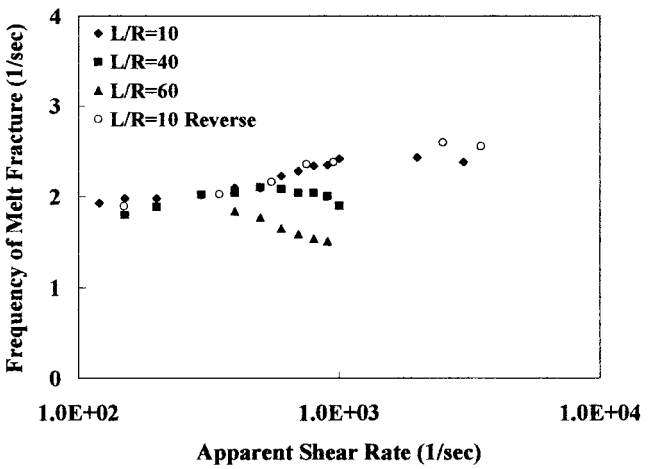

Figure 8 The frequency of the regular melt fracture versus the apparent shear rate.

After the critical stress, the melt fracture occurred as periodical patterns. The wavelength increased when the shear rate increased. This can be seen in Figure 1. The ratio between the wavelength and average melt flow rate in the capillary represented the frequency of oscillation. The die swell data in Figure 7 were used to adjust the flow rate of the extrudate to the capillary flow rate. Figure 8 shows the frequency of the regular melt fracture versus the true shear rate. The frequency was on the order of 1 s^{-1} and was found to be almost independent of the shear rate. The onset of regular melt fracture was slightly delayed when high L/D dies were used. This agreed with the observation of Baik and Tzoganakis.[19] It has been reported that, during the spurt stage, the frequency of pressure oscillation of PE increased when the amount of polymer in the barrels decreased.[3,9–11] However, the appearance of sharkskin was not related to the barrel volume.[9] To verify any barrel size dependence, another run was made on the die with $L/R = 10$, starting from a high shear rate to a lower one. It was found that the wavelength and frequency agreed with the results measured from low plunger speed to high speed. This indicated that the mechanism creating regular melt fracture of PP was independent of barrel size. It was observed that the frequency decreased slightly when the capillary length increased. This indicated that, in the longer die, more relaxation processes took place and the melt fracture reached an asymptotic state. From these observations, the regular melt fracture seemed to be related to strain at the die inlet or outlet, which relaxed to a constant value for a long die and was independent of the barrel size.

The average value of the frequency was estimated to be 2 s^{-1}. For comparison, the data of Atofina 3622 was also calculated by the same approach. The melt fracture with a regular melt fracture pattern was observed only at the highest shear rate.[18] The frequency was estimated to be 18 s^{-1} for $L/R = 40$ and 12 s^{-1} for $L/R = 60$. These numbers are higher than the results for PP 3181. A shorter die also had a higher frequency in Atofina 3622. The results of Atofina 3622 were measured at an apparent shear rate of 5000 s^{-1}. If the trend of the largest die in Figure 7 continued, it could be concluded that Atofina 3181 had a longer wavelength and lower frequency than Atofina 3622. This may be attributed to a difference in the molecular weight and melt viscosity. Because both PPs had similar critical shear stress, the factors determining the wavelength of the melt fracture appeared to be different than those determining the onset of the melt fracture. This issue deserves future study.

CONCLUSIONS

Melt fractures of a high molecular weight PP were observed in a capillary rheometer. The flow curve and extrudate appearance could be divided into three regions. At the low flow rate, smooth extrudate was obtained. At the next stage, a melt fracture with regular patterns was observed. The frequency of the regular melt fracture was independent of the barrel volume and shear rates, but it decreased when the die length increased. An equation including the pressure effect on the shear viscosity and extensional viscosity was used to calculate the wall shear stress and end effect. The shear viscosity and extensional viscosity were calculated and correlated well with another low molecular weight PP.

The authors would like to express their special thanks to Dr. R. D. Deanin of the Department of Plastics Engineering at the University of Massachusetts Lowell for his invaluable help and useful discussions.

References

1. Sornberger, G.; Quantin, J. C.; Fajolle, R.; Vergnes, B.; Agasant, J. F. J Non-Newtonian Fluid Mech 1987, 23, 123.
2. Ramamurthy, A. V. J Rheol 1986, 30, 337.
3. Kalika, D. S.; Denn, M. M. J Rheol 1987, 31, 815.
4. Larson, R. G. Rheol Acta 1992, 31, 2130.
5. Denn, M. M. Annu Rev Fluid Mech 1990, 22, 13.
6. Shore, J. D.; Ronis, D.; Piche, L.; Grant, M. Phys Rev Lett 1996, 77, 655.
7. Weill, A. Rheol Acta 1980, 19, 623.
8. Hatzikiriakos, S. G. Polym Eng Sci 1994, 34, 1441.
9. Hatzikirakos, S. G.; Dealy, J. M. J Rheol 1992, 36, 845.
10. McLeish, T. C. B.; Ball, R. C. J Polym Sci Polym Phys Ed 1986, 24, 1735.
11. Becker, J.; Bengtsson, P.; Klason, C.; Kubat, J.; Saha, P. Int Polym Proc 1991, 6, 318.
12. Ui, J.; Ishimaru, Y.; Murakami, H.; Fukushima, N.; Mori, Y. SPE Trans 1964, 295.
13. Ballenger, T. F.; Chen, I.; Crowder, J. W.; Hagler, C. E.; Bogue, D. C.; White, J. L. Trans Soc Rheol 1971, 15, 195.
14. Bartos, O. J Appl Phys 1964, 35, 2767.

15. Kamide, K.; Inamoto, Y.; Ohno, K. Int Chem Eng 1966, 6, 340.
16. Akay, G. J Non-Newtonian Fluid Mech 1983, 13, 309.
17. Fujiyama, M.; Kawasaki, Y. J Appl Polym Sci 1991, 42, 467.
18. Huang, J. C.; Leong, K. S. J Appl Polym Sci 2002, 84, 1269.
19. Baik, J. J.; Tzoganakis, C. Polym Eng Sci 1998, 38, 274.
20. Kazatchkov, I. B.; Hatzikiakos, S. G.; Stewart, C. W. Polym Eng Sci 1995, 35, 1864.
21. Penwell, R. C.; Porter, R. S.; Middelman, S. J Polym Sci A-2 1971, 9, 731.
22. Huang, J. C.; Shen, H. F. Adv Polym Tech 1989, 9, 211.
23. Huang, J. C.; Liu, H.; Liu, Y. Polym Plast Tech Eng 2001, 40, 79.
24. Denn, M. M. Polym Eng Sci 1981, 21, 65.
25. Binding, D. M.; Couch, M. A.; Walters, K. J Non-Newtonain Fluid Mech 1998, 79, 137.
26. Christensen, J. H.; Kjaer, E. M. SPE ANTEC 1998, 985.
27. Bagley, E. B. J Appl Phys 1957, 28, 624.
28. Cogswell, F. N. Polym Eng Sci 1972, 12, 64.
29. Piau, J. M.; El-Kissi, N.; Tremblay, B. J Non-Newton Fluid Mech 1988, 30, 198.
30. Gupta, R. K. Polymer and Composites Rheology, 2nd ed.; Marcel Dekker: New York, 2000; Chapter 3.
31. Van Krevelen, D. W. Properties of Polymers, 2nd ed.; Elsevier: New York, 1976.
32. Ferry, J. D. Viscoelastic Properties of Polymers, 3rd ed.; Wiley: New York, 1980.
33. Tzoganakis, C.; Vlachopoulos, J.; Hamielec, A. E.; Shinozaki, D. M. Polym Eng Sci 1989, 29, 390.
34. Zoller, P.; Walsh, D. Standard Pressure–Volume–Temperature Data for Polymers; Technomic: Lancaster, PA, 1995.
35. Vlachopoulos, J. Revu Deform Behav Mater 1981, 3, 219.
36. Brandao, J.; Spieth, E.; Lekakou, C.; Polibrasil, S. A. Polym Eng Sci 1996, 36, 49.